Stereoselectivity by Enantiomeric Inhibitors of Matrix Metalloproteinase-8: New Insights from Molecular Dynamics Simulations

Massimiliano Aschi,[†,*] Neva Besker,[‡] Nazzareno Re,[‡] Giorgio Pochetti,[§] Cecilia Coletti,[‡] Carlo Gallina,[‡] and Fernando Mazza[†,§,*]

Dipartimento di Chimica, Ingegneria Chimica e Materiali, Università di L'Aquila, Italia, Dipartimento di Scienze del Farmaco, Università "G. d'Annunzio", Chieti, Italia, and Istituto di Cristallografia, C. N. R., Monterotondo Stazione, Rome, Italy

Received July 19, 2006

Molecular Dynamics simulations in aqueous solution were performed for the matrix metalloproteinase-8 (MMP-8) free catalytic domain and for its complexes with the (*R*)- and (*S*)-[1-(4′-methoxybiphenyl-4-sulfonylamino)-2-methylpropyl] phosphonate. The 144−155 loop of the enzyme undergoes a drastic decrease of mobility once complexed with both enantiomers. The two enantiomers induce a different decrease of conformational entropy upon complexation. The higher affinity of the *R*-enantiomer can be related to the lower loss of conformational entropy accompanying its binding. The differences in the dynamical behavior of the protein induced by the two enantiomers are discussed at molecular level and the mode of binding of the simulated complexes is compared with that previously determined by X-ray crystallography.

Introduction

Matrix metalloproteinases (MMPs) are zinc endopeptidases capable of cleaving the proteins of the extracellular matrix. These enzymes are involved in several physiological processes such as angiogenesis, embryogenesis, differentiation, and wound healing.[1,2] Excessive levels of their activity, however, are responsible for an uncontrolled matrix degradation in a variety of pathological states such as multiple sclerosis,[3−6] osteoarthritis,[7] rheumatoid arthritis,[8,9] osteoporosis,[10,11] Alzheimer's disease,[12] and tumor growth and metastasis.[13−15]

The development of synthetic inhibitors modulating MMP activity is one approach[16−19] for the treatment of these degenerative pathologies. A great variety of synthetic, low molecular weight MMP inhibitors have been prepared and their binding to MMPs has been determined by X-ray crystallography and NMR spectroscopy.[20−32] Their structures include a peptide or a peptidomimetic moiety generally accommodated in the S′ region of the active site and a zinc-binding group (ZBG) capable of coordinating the catalytic zinc ion. Although hydroxamate is considered the most effective ZBG, hydroxamate inhibitors have generally low specificity because of the overwhelming contribution of the hydroxamic group to binding, show poor pharmacokinetic properties, and may cause toxic effects in long-term treatment owing to the release of hydroxylamine, a well-known carcinogenic compound. Therefore, MMP inhibitors based on less potent zinc-binding functions, such as carboxylate, phosphonate, and thiolate, are also currently investigated. In accordance with these considerations, we have been studying phosphonate MMP inhibitors for a long time, with the aim of obtaining new potent and selective analogues, endowed with a more favorable pharmacokinetic profile with respect to hydroxamates.[33−37] Following our interest in this field, we recently prepared the *R*- and *S*-enantiomers of [1-(4′-methoxybiphenyl-4-sulfonylamino)-2-methylpropyl] phosphonate and solved the crystal structure of their complexes with the catalytic domain of MMP-8.[37] Both enantiomeric forms, similarly to analogous carboxylates and hydroxamates,[38,39] are effective MMP inhibitors. However, the *R* enantiomer shows a much higher inhibiting activity ($K_i = 0.6 \pm 0.14$ nM)[37] with respect to the *S* isomer ($K_i = 700 \pm 190$ nM).[37]

Figure 1 shows a ribbon-type plot of MMP-8 that exhibits a spherical shape, with a shallow active site cleft separating the bigger upper N-terminal domain from the smaller lower C-terminal domain. The upper domain consists of a central highly twisted five-stranded β-pleated sheet and two long α-helices including the active site helix containing the two zinc-binding histidine and catalytic glutamic acid residues of the H197-E198-Xaa-Xaa-H201 zinc-binding motif. The key inhibitor- and substrate-binding residues in the upper domain comprise residues L160−F164 of the "edge" strand positioned above the active site helix and the "bulge" segment G155−L160. The catalytic zinc ion is situated at the bottom of the active site cleft and is coordinated to the N^{ϵ} imidazole atoms of the three histidine residues delimiting the consensus motif HEXXHXXGXXH.

Common features of the binding of both enantiomeric inhibitors to this active site found in the crystal[37] are occupation of the primed region of the active site, coordination of the catalytic zinc ion by the phosphonate group, and insertion of the biphenyl substituent into the deep primary specificity pocket S_1'. The two enantiomers, however, adopt different conformations of the sulfonamide junction and of the lengthy biaryl system.

On the basis of these crystallographic investigations, the higher inhibiting activity of the *R*-enantiomer was mainly related to the presence in its complex of a direct inhibitor to enzyme H-bond of the sulfonamide NH, replacing a water-mediated H-bond in the *S*-isomer complex, and to more extensive π-stacking interactions, involving both phenyl rings of the *R*-isomer.[37]

For a better comprehension of the enzyme−ligand binding interactions occurring in aqueous solution, the biological medium where binding affinities have actually been determined, we performed MD simulations of the fully hydrated enzyme[40] and its two complexes. In particular, our aim is to shed light on the factors determining the stereoselective inhibition of

* Corresponding authors. M.A., e-mail: aschi@caspur.it, tel +39-0862-433775, fax +39-0862-433753. F.M., e-mail: mazza@univaq.it, tel +39-0862-433768, fax +39-0862-433753.

† Dipartimento di Chimica.

‡ Dipartimento di Scienze del Farmaco.

§ Istituto di Cristallografia.

10.1021/jm0608457 CCC: $37.00
Published on Web 12/22/2006

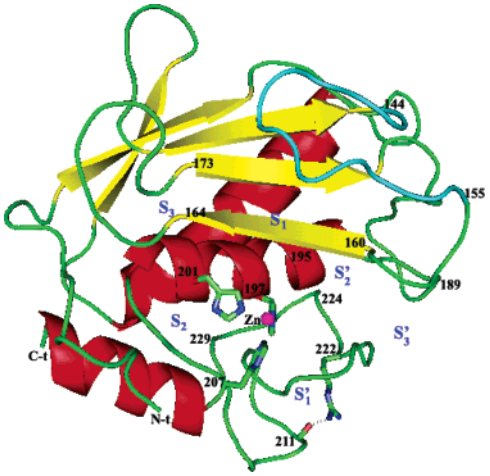

Figure 1. Ribbon-type plot of MMP-8. Helices, β-strands, and unstructured regions are represented by ribbons, arrows, and ropes, respectively. The catalytic zinc ion and the coordinated H197, H201, and H207 are explicitly represented, as well as the S3−S3′ subsites of the active site. The loop 144−155 is colored in cyan.

MMP-8 by the considered enantiomeric pair model. It has become clear in recent years that molecular recognition processes are tightly dependent on the dynamical properties of the molecular systems.[41] In this context, Molecular Dynamics (MD) simulations can provide substantial insights for evaluating local and global impact of binding and pointing out key protein−ligand interactions.[42] Moreover, by examining the motion of a free and ligated protein it is possible to evaluate the various physical effects contributing to free energy, including individual enthalpic terms and conformational energy variations which have recently been recognized to be of crucial importance for ligand binding.[41,43] Our MD results show that the higher affinity of the *R*- relative to the *S*-enantiomer can be related to the lower conformational entropy penalty accompanying the complexation of the *R*-phosphonate.

Computational Methods

MMP-8 catalytic domain and its complexes with the *R*- and *S*-enantiomer of [1-(4′-methoxybiphenyl-4-sulfonylamino)-2-methylpropyl] phosphonate have been investigated in aqueous solution through MD techniques using the GROMACS[44] package. Each system was initially placed in a rectangular box of 125 nm^3 with 3787 water molecules, described by the single point charge (SPC),[45] and seven counterions (Na^+). The dimension of the box was selected in order to avoid any interaction of the solute with its replica, which could arise from the application of periodic boundary conditions. Rototranslational constraints were applied to the solute for obtaining correct statistical mechanics and thermodynamics.[46] The same initial coordinates, taken from the MMP-8:*S*[37] crystal complex (PDB code 1ZS0), were adopted for the enzyme in the three systems.

The reason for this choice lies in the fact that in a MD simulation of the *R*-complex starting from the MMP-8:*R* crystal structure coordinates (PDB code 1ZVX),[37] the enzyme, although undergoing the same conformational transitions, unfolded after approximately 12 ns. Furthermore, by adopting the MMP-8:*S* crystal coordinates for the enzyme, we were able to evaluate the effect of the complexation on the stability of the R222 N^{η} ···P211 CO hydrogen bond, which is present only in MMP-8:*S* crystal complex.

In the simulation of the free enzyme, one water molecule, replacing the ligand, was linked to the zinc ion. For the simulations of the two complexes, each enantiomer was inserted in a position as close as possible to that found in the crystal complex. All the systems were initially minimized by using a standard steepest descent algorithm. Then, after solvation and the initial equilibration of the solvent, each system was relaxed for 100 ps in an isothermal/isobaric ensemble to obtain the correct density of water. Each simulation was finally carried out in an isothermal/isochoric ensemble at 300 K for 15.0 ns using an integration step of 2.0 fs. Only the last 11.0 ns of each trajectory, containing stationary values of the C^{α} root-mean-square deviations, were analyzed. The temperature was kept constant by the isokinetic temperature coupling.[47] All bond lengths were constrained using LINCS.[48] The long-range electrostatics was computed by the Particle Mesh Ewald method,[49] with 34 wave vectors in each dimension and a fourth order cubic interpolation.

Gromos force field[50] parameters were adopted for the enzyme, while the Lennard−Jones parameters of similar atoms were considered for the inhibitors. The point charges of the inhibitors were calculated by a fitting procedure[51] using a DFT calculation with Becke's three-parameter exchange and the Lee, Yang, and Parr correlation functionals (B3LYP)[52] with the 6-311++G(p,d) basis set. The torsion angle parameters were obtained using the same level of theory. The reliability of the force field parameters was checked by reproducing the DFT absolute minimum *in vacuo*. All quantum chemical calculations were performed using the Gamess package.[53]

Essential Dynamics (ED) analysis[54] of the trajectories of atomic coordinates was employed to point out the conformational changes. This method consists of building the covariance matrix of the atomic positional fluctuations obtained from MD simulations. After its diagonalization, an orthonormal set of vectors (eigenvectors) defines a new set of generalized coordinates along which the fluctuations occur. The eigenvectors with the largest eigenvalues allowed us to define the essential subspace in which to search for the free energy minima. In our case, the essential plane, defined by the first two eigenvectors, was divided into a grid of 20 × 20 square cells, onto which the trajectories were projected. The free energy difference between two cells (i and j) can be evaluated by the equation

$$\Delta A_{i\rightarrow j} = -k_B T \ln (p_j/p_i)$$

where k_B is the Boltzmann constant and p_i and p_j represent the probability to find the projected trajectory onto the "i" and "j" cell, respectively.

An estimate of the differential binding affinity of the two inhibitors toward MMP-8 was carried out as follows. Let us consider the reaction E + I = EI + $\Delta\mu^{\circ}_{EI,}$ where the inhibitor I reversibly reacts with the enzyme E, $\Delta\mu^{\circ}_{EI}$ is the standard free energy variation for the formation of the complex EI. If $\Delta\mu^{\circ}_{ER}$ and $\Delta\mu^{\circ}_{ES}$ are the molar free energy variations for the formation of the *R*- and *S*-enantiomer complexes with MMP-8, respectively, the differential binding affinity is $\Delta\Delta\mu^{\circ}_{S-R} = \Delta\mu^{\circ}_{ES} - \Delta\mu^{\circ}_{ER}$. As described below, the two free enantiomers show essentially the same RMSFs in solution. This similarity allows us to assume, as a first approximation, the same chemical potentials for the free inhibitors in water. It follows that the differential binding affinity can be considered very close to the difference between the chemical potentials of the two complexes ($\Delta\Delta\mu^{\circ}_{S-R} \cong \mu_{ES} - \mu_{ER}$). To evaluate this difference, the configurational integrals of the two complexes, Q_S and Q_R, have been computed. Assuming no large differences in the solvation contributions, and due to the absence of excited electronic states and to the negligible variation in the shape of the two complexes (i.e. same mass tensor determinants), it is possible to include for each complex the vibrational term only. We have taken into account the eigenvalues (ω^2) of the covariance matrix, which provides the variance along the eigenvectors. In the harmonic approximation and according to the equipartition theorem, the contribution of each i-th oscillator to the energy is given by 1/2 κ_i ω^2 where $\kappa_i \cong k_B T/\omega^2$. The ratio of the configurational integrals (Q_S/Q_R) is thus equal to the ratio of the square root of the determinants of the corresponding covariance matrices. We have therefore evaluated the backbone covariance matrix again, including also the inhibitors atoms.

Results and Discussion

Simulation of the Uncomplexed Enzyme. The qualitative structural behavior of the protein, together with the stability of

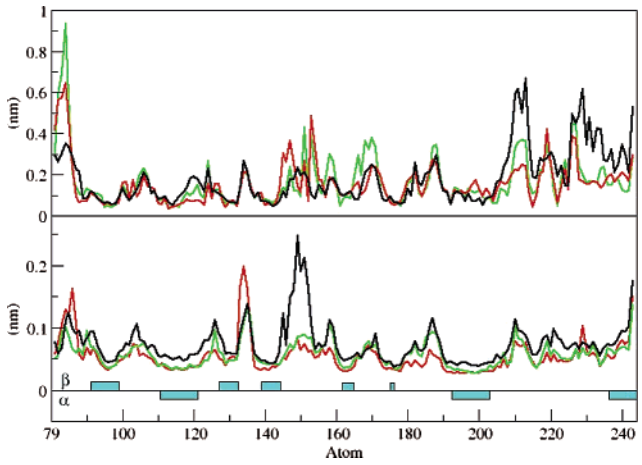

Figure 2. Root-mean-square deviations (rmsd, upper panel) of the MMP-8 C^{α} atoms of the free enzyme (black curve) and of the enzyme complexed with the *R*- (green curve) and *S*-enantiomer (red curve) with respect to the crystal structure. In the lower panel root-mean-square fluctuations (RMSF) are reported for the same systems. The cyan blocks above and below the baseline indicate β-strand and helix regions, respectively.

the simulations, has been investigated by calculating the root-mean-square deviations (RMSDs) of the C^{α} atoms of the free and both complexed enzyme with respect to the initial crystal structure (Figure 2, upper panel). Comparison of this figure with the root-mean-square fluctuations (RMSFs) plot for the same systems (Figure 2, lower panel) shows that the largest deviations and fluctuations occur in the unstructured regions, while α and β regions remain essentially unaltered along the simulations. It is interesting to remark that a slightly different root-mean-square fluctuation profile can be observed for the two complexes. In particular, the complex with the *R*-enantiomer shows a fluctuation pattern distributed along a larger number of residues. A quantitative evaluation of the internal mobility of the three systems was achieved by using ED analysis carried out by diagonalizing the covariance matrix of the backbone fluctuations. Figure 3 reports a significant portion of the covariance matrix spectrum of eigenvalues for the free MMP-8 and the two complexes. The trace of the diagonalized covariance matrix (i.e. the sum of the eigenvalues) of the free enzyme is larger than that of both complexes (1.52 nm^2, 0.76 nm^2, and 0.60 nm^2 for the free enzyme, *R*- and *S*-complex, respectively) and indicates that the overall enzyme flexibility decreases upon complexation. This is particularly remarkable in the region 144−155. As shown in Figure 1, this region belongs to the S-shaped loop connecting the S_{III} to S_{IV} strand and leads to the "bulge" segment bordering the right-hand side of the active site.[55] A similar behavior, although involving a smaller number of residues and at a weaker extent, was already noted in shorter MD simulations performed for MMP-8 alone and in the presence of a ligand interacting alternatively with the primed or the unprimed region of the active site.[40]

On the basis of the ED analysis, we also examined in detail the backbone conformational changes. Figure 4 shows the backbone conformations corresponding to the three almost degenerate free energy minima obtained from the projection of the trajectory of the uncomplexed enzyme onto the essential plane defined by its first two eigenvectors (see Computational Methods). The sharp fluctuation of the 144−155 loop of the free MMP-8 can be described as a "gate-like" motion with a frequency of approximately 1.2 ns^{-1}. This motion completely disappears whenever the ligand is bound to the active site. This inhibitor-induced conformational change in the MMP-8 S-shaped loop indicates that the binding of the inhibitor leads to local structural alterations as well as to significant long-range localized conformational changes stabilizing the complex.

Simulation of the Complexes: Interactions Outside the S_1' Subsite. The binding interactions resulting from the MD simulations performed on the fully hydrated complexes are schematically reported in Figure 5. Both enantiomers maintain the important polar interactions outside the S_1' subsite. Two phosphonate oxygens coordinate the catalytic zinc ion in a bidentate mode (Zn···O distances in the range 0.22−0.28 ± 0.01 nm), while the third oxygen is always H-bonded to an exchanging water molecule. One of the sulfonyl oxygens anchors both inhibitors to the upper rim of the active site by H-bonding the A161 NH group. A further H-bond is formed by the *R*- and *S*-enantiomer sulfonamide NH with the side-chain E198 and the backbone A161 CO groups, respectively. This situation is achieved through different rotations around the dihedral angles formed by zinc binding group (P−C−N−S) and the sulfonamide junction (C−N−S−C). The average values for these angles obtained by MD simulations are −170° ± 15°, 122° ± 10° for the *R*- and 52°± 8°, 53° ± 8° for *S*-enantiomer, while the corresponding values found in the crystal complexes MMP-8:*R* and MMP-8:*S*[37] are −121°, 72° and 108°, −89° respectively. The significant difference between the crystal structures and MD simulations in the torsion angle of *S*-enantiomer sulfonamide junction corresponds to the different g^+ conformation adopted by the fully hydrated complex in the simulation.

Interactions Inside the S_1' Subsite. The biphenyl group of both enantiomers, occupying the primary specificity S_1' subsite, plays a crucial role in binding, and its orientation seems determinant for the stereoselectivity. In order to evaluate the differences induced by the binding, the RMSFs of the enzyme and of the complexed and free inhibitors were analyzed. Figure 2 shows that the fluctuations of the unstructured regions around the S_1' subsite are larger when the enzyme is complexed with the *R*- rather than the *S*-isomer. Moreover, while the largest fluctuations of the enzyme in the complex with the *S*- isomer are basically localized on the first eigenvector only, in the complex with the *R*-isomer they also involve the second eigenvector (see Figure 3). The larger internal mobility of the complex with the *R*-isomer may be highlighted by different eigenvalues spectra. Atomic RMSFs of the complexed inhibitors are reported in Figure 6 and compared with those of the free inhibitors in aqueous solution. While the two enantiomers maintain a similar profile for the moieties interacting outside the S_1' subsite (atoms 1−15 in Figure 6), the relative mobility of the biphenyl group (atoms 25−36 in Figure 6) in the *R*-isomer is significantly larger than in the *S*-isomer and only slightly smaller than in the free inhibitor. This suggests that the conformational space accessible to the complexed *R*-isomer is larger than that sampled by the *S*-isomer. In order to describe the inhibitor conformational changes, their positional fluctuations were analyzed by ED, with the same procedure previously adopted for the free enzyme. The corresponding trajectories, projected onto the related essential plane, are reported in Figure 7 and Figure 8. In these figures the regions of the essential space corresponding to the most stable conformations are highlighted by dots. Such conformations are also schematically reported as superimposed to the crystal conformations.[37] From Figure 7 it is evident that the biphenyl group of the *S*-isomer is tightly bound inside the S_1' subsite, where it samples a single free energy minimum corresponding to the conformation characterized by an average torsion angle (τ) around the two phenyl rings

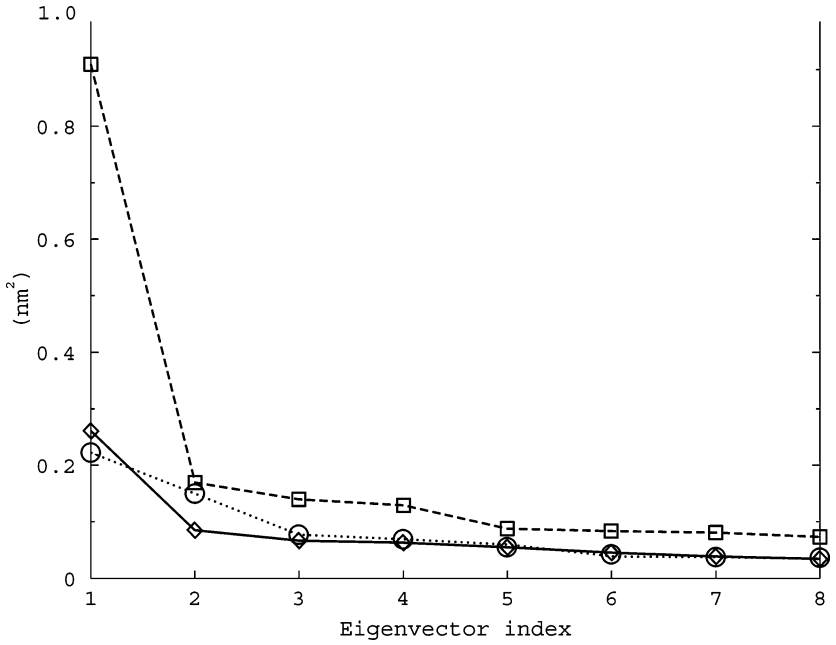

Figure 3. Eigenvalues (nm^2) obtained from diagonalization of the covariance matrix of the MMP-8 backbone positional fluctuations for the free enzyme (squares) and after complexation with the *R*- (circles) and *S*-enantiomer (diamonds).

Figure 4. A picture of the 'gate-like' motion adopted by the 144−155 loop of the free enzyme during the simulation. The red, green, and blue loops represent the backbone conformations corresponding to the free energy minima (see text). The rest of the enzyme backbone is reported in gray. The purple sphere represents the catalytic zinc ion.

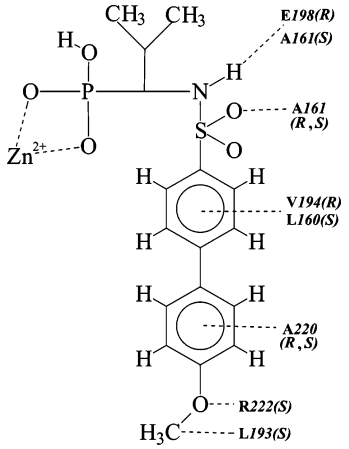

Figure 5. Schematic representation of the main binding interactions resulting from the MD simulation of the two enantiomers in the active site of MMP-8. (*R*) and (*S*) indicate the enzyme residues involved by the *R*- and *S*-enantiomer, respectively. (*R*, *S*) indicates that the same residue is involved in both complexes.

of 40° ± 8°. This conformation is constrained by the following interactions (see Figure 5): (i) a polarization interaction between the π-cloud of the inhibitor proximal phenyl ring and the L160 methyl (0.29 ± 0.02 nm); (ii) a H-bond between A220 NH and the distal phenyl ring (0.32 ± 0.03 nm); (iii) an additional H-bond (0.27 ± 0.01 nm) between the methoxy oxygen and the R222 N^{η}, and (iv) hydrophobic interactions between the methoxy group of the inhibitor and L193 side chain (0.39 ± 0.04 nm). On the other hand, two essentially degenerate interconverting free energy minima were found onto the essential plane for the biphenyl group of the *R*-isomer (Figure 8). The conformations of these two minima are characterized by average torsion angles (τ) of 60° ± 10° and 30° ± 6°, respectively. It should be noted that both conformations are stabilized by the A220 NH group which alternatively H-bonds the π-cloud of the distal phenyl ring (0.36 ± 0.03 nm) when $\tau = 60°$, or the methoxy oxygen (0.35 ± 0.03 nm) when $\tau = 30°$.

The R222 residue plays a crucial role in the different behavior of the two inhibitors. The examination of the MMP-8 crystal complexes, available from Protein Data Bank, shows that the R222 N^{η}, lying on the loop delimiting the lower part of the S_1' subsite, is generally involved in an intramolecular H-bond with either the P211, or G212, or A213 residue, all belonging to the facing loop. These two loops separate the crevice harboring the inhibitor biphenyl group from bulk water.

In the MMP-8:*S* crystal the R222 N^{η} and P211 CO groups are able to form one H-bond (0.27 nm), whereas these groups are 0.38 nm apart in the MMP-8:*R* crystal. Because of this difference, in the MD simulation of the complexes we have monitored the R222 N^{η} ···P211 CO distance, whose average value was found equal to 0.29 ± 0.05 nm and 0.49 ± 0.07 nm for the *S*- and *R*-isomer complexes, respectively (Figure 9).

The binding of the *S*-inhibitor preserves the R222 N^{η}···P211 CO H-bond, keeping the walls of the S_1' subsite fastened, lowers the local enzyme mobility, and hinders entry of bulk water. On the contrary, binding of the *R*-inhibitor causes the break-up of the R222N^{η}···P211CO H-bond, facilitates the opening of the S_1' subsite favoring local higher mobility and exchange of bulk

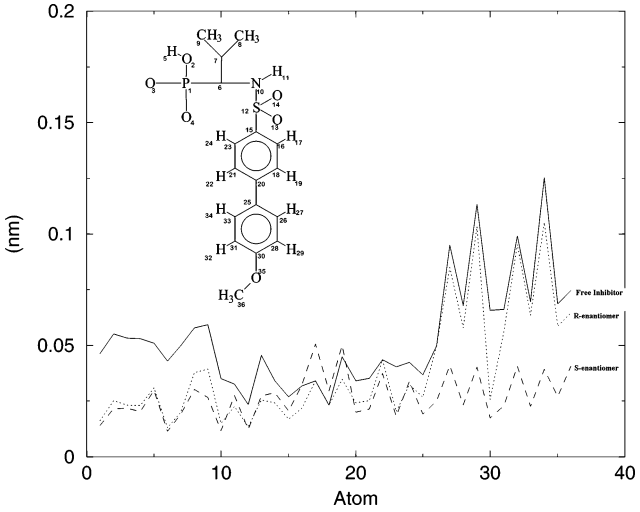

Figure 6. RMSFs (nm) of the inhibitor atoms. Atom numbers are reported in the formula. Methyl groups were treated as single atoms. Dotted and dashed lines represent the *R*- and *S*-enantiomer complexes, respectively. The solid line represents both free enantiomers in aqueous solution.

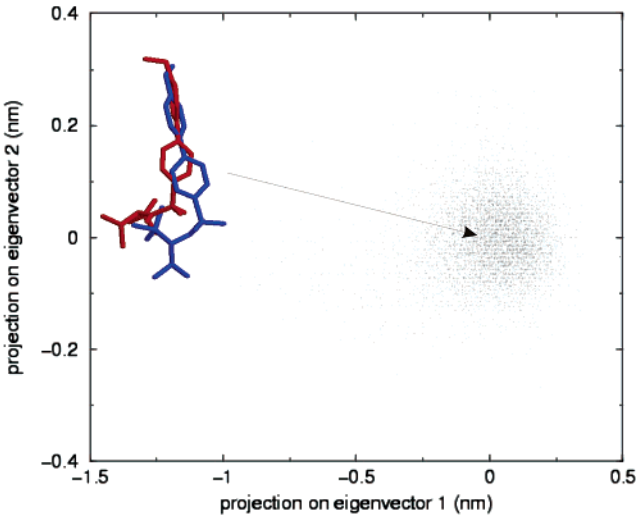

Figure 7. Projection of the trajectory onto the essential plane of the simulated *R*-complex. The free energy minima conformations (red) are superimposed to that found in the crystal structure of MMP-8:*R* (blue).[37]

water. To support the latter conclusion, we have examined the number of water molecules within the S_1' subsite of the two complexes. Figure 10 shows the time course of the number of water molecules included in the space between the inhibitor and the closest atoms of the wall subsite. It can be noted that the *R*-enantiomer complex shows a higher degree of hydration being the average number of water molecules 10 ± 1, against a value of 7 ± 1, found for the complex with the *S*- enantiomer.

Rigid-Body Motion of the Biphenyl Group. In addition to the inhibitor internal fluctuations, the rigid-body fluctuations of the biphenyl group into the S_1' pocket present interesting features. The rigid-body motion was referred to an internal rigid orthogonal frame chosen as follows (see inset of Figure 11). The origin is placed on the catalytic zinc ion. The $\boldsymbol{\xi}$ unit vector points to the N^{ϵ} atom of H197. The $\boldsymbol{\lambda}$ unit vector, lying in the plane of the zinc ion and of the N^{ϵ} atoms of H197 and H207 residues, is perpendicular to $\boldsymbol{\xi}$. Finally, the $\boldsymbol{\eta}$ unit vector is perpendicular to the ($\boldsymbol{\xi}$, $\boldsymbol{\lambda}$) plane. The origin of unit vector $\boldsymbol{\rho}$, along the 2-fold axis of the biphenyl group, is set on the S atom of the inhibitor. Figure 11 reports the φ and ψ angles formed by $\boldsymbol{\rho}$ with $\boldsymbol{\xi}$ and $\boldsymbol{\eta}$, respectively. The dotted gray and black areas

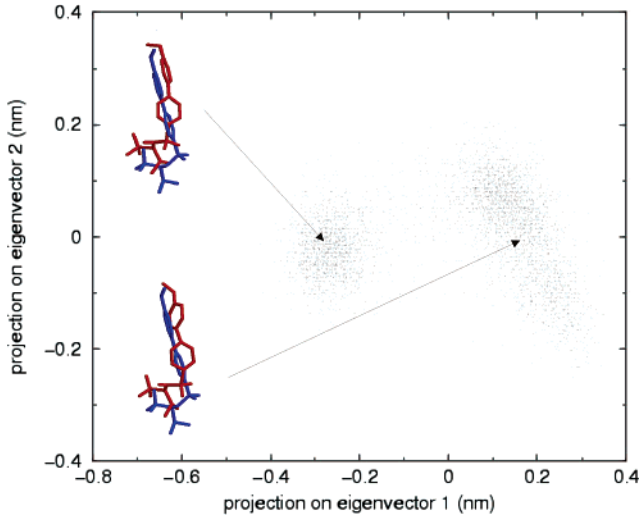

Figure 8. Projection of the trajectory onto the essential plane of the simulated *S*-complex. The free energy minimum conformation (red) is superimposed to that found in the crystal structure of MMP-8:*S* (blue).[37]

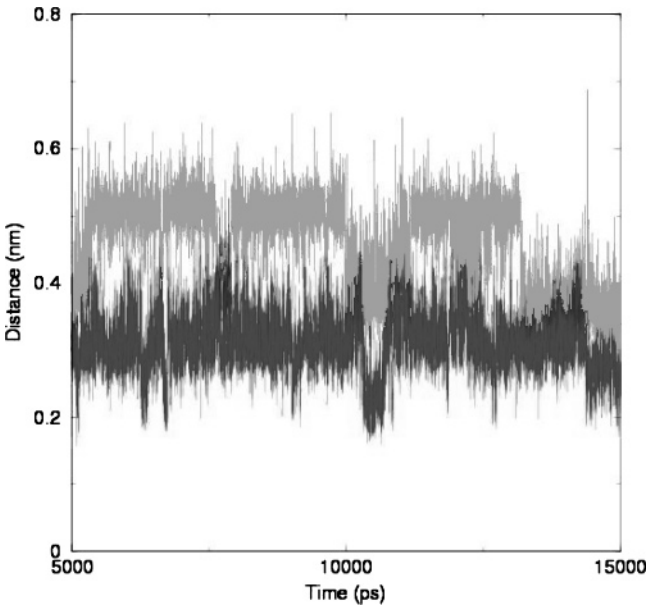

Figure 9. Time course of the MMP-8 R222 $N^{\eta}\cdots$P211 CO contact distance (nm) for the *R*- (gray curve) and *S*-enantiomer (black curve) enzyme complexes. The behavior for the free enzyme is practically identical to that shown by the black curve.

represent the values sampled by the *R*- and *S*-enantiomer, respectively, while gray and black crosses indicate the values found in the MMP-8:*R* and MMP-8:*S* crystal complexes, respectively. While the orientation of $\boldsymbol{\rho}$ observed in the crystal structure of the *S*-isomer falls in the black area, the *R*-isomer undergoes a rigid-body transition and the crystal value is never sampled during the simulation. The biphenyl orientation observed in the MMP-8:*R* crystal, although adopted as the starting point in the simulation, is abandoned within the first 20 ps. (The same behavior was observed when the simulation was initiated with the MMP-8:*R* crystal coordinates). Within the same interval, breaking of the R222 $N^{\eta}\cdots$P211 CO H-bond also takes place. These concerted events seem important for the different binding affinity of the two inhibitors.

The disagreement between MD simulations and crystallographic investigations is only apparent. In fact, MD simulations have been performed on the fully hydrated systems at room temperature. These conditions favor the molecular motions, as

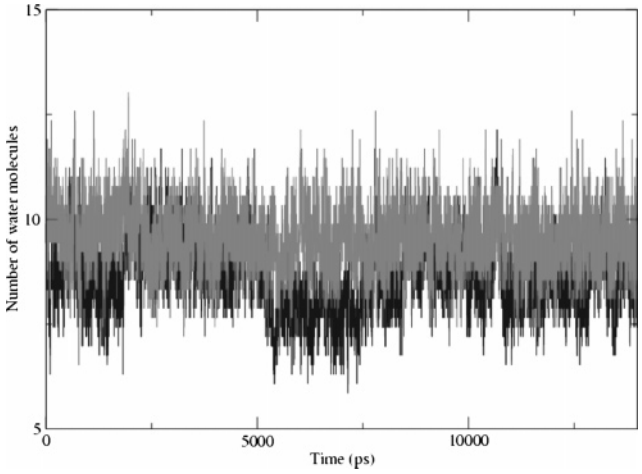

Figure 10. Time course of the number of water molecules within the $S_{1'}$ subsite for the *R*- (gray curve) and *S*-enantiomer (black curve) complexes.

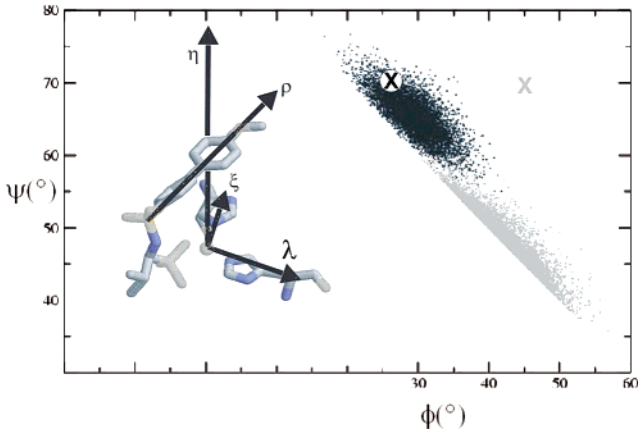

Figure 11. Orthogonal reference frame ($\boldsymbol{\xi}$, $\boldsymbol{\lambda}$, and $\boldsymbol{\eta}$ unit vectors) for the rigid-body motion of the biphenyl group (inset), and plot of the φ and ψ angles (degrees) formed by the unit vector $\boldsymbol{\rho}$ with $\boldsymbol{\xi}$ and $\boldsymbol{\eta}$. Dotted gray and black areas, respectively, represent the biphenyl orientation on the φ/ψ plane adopted by the *R*- and *S*-enantiomer during the simulations. Gray and black crosses indicate the orientation found in the crystal MMP-8:*R* and MMP-8:*S* complexes, respectively.

can be argued from the increase of the gyration radius during the simulation of the fully hydrated protein with respect to the initial crystal coordinates. On the other hand, X-ray investigations were performed on the crystal complexes with diffraction data collected at 100 K. The crystals were obtained from dilute solutions of the complexes, by progressively removing water molecules to get the saturation conditions. For this reason, it seems probable that the breaking of the R222 $N^{\eta}\cdots$P211 CO H-bond, observed in the crystal MMP-8:*R* only, occurs in aqueous solution and is maintained during the crystal formation. As a matter of fact, the two crystal complexes differ for unit cell parameters and crystal packings.

In conclusion, the present analysis clearly indicates a drastic decrease of fluctuations for the two systems upon complexation. The decrease is less pronounced, both for the enzyme and inhibitor, when the *R*-isomer is complexed. This is apparently the most important difference between the two systems, and it can be interesting to investigate if, and to what extent, it might reflect the different stability of the two complexes. This has stimulated us to investigate the differential binding affinity, as reported in the next section.

Binding Affinity Estimation. The inhibiting activity against MMP-8 of the *R*-isomer ($K_i = 0.6 \pm 0.14$ nM) is about 1000-fold larger than that of the *S*-isomer ($K_i = 700 \pm 190$ nM).[37] The differential binding affinity of the two inhibitors can be estimated on the basis of the MD simulations, although it represents nowadays one of the most challenging and difficult tasks of computational chemistry.[56−60] In this study we provide an estimate of the differential binding affinity which, however, because of the several approximations (see Computational Methods), has a semiquantitative value only. At 300 K, we obtained a ratio between the complexation equilibrium constants involving the *R*- and *S*-inhibitor, K_R/K_S, equal to 64. This value is about 1 order of magnitude smaller than the ratio between the measured K_is.[37] Such a discrepancy is probably due to the inclusion of several approximations in the model and to the limited simulation time, which obviously prevent a more quantitative estimation. Nonetheless, our result clearly indicates a larger affinity of the *R*-isomer for MMP-8. Moreover, the contribution of the internal energy, taken as the difference between the average values of the potential energy along the simulations, is the same within the noise. This is again a confirmation that the use of the same starting coordinates to model the enzyme in both complexes does not lead to a destabilized system. More important, as a consequence of the similar internal energy for the two systems, the present analysis suggests that the larger affinity of the *R*-isomer can be ascribed only to the larger conformational entropy shown by its complex, which is consistent with the higher conformational flexibility and the higher water mobility within the S_1' subsite as revealed by the detailed analysis of the MD trajectories (see above).

The importance of conformational entropy in contributing to the stability of ligand−protein complexes has been shown for several systems.[41,43] In particular, isothermal titration calorimetry[38] was recently employed to analyze the binding thermodynamics of the enantiomeric inhibitors *R*- and *S*-2-[4′-bromobiphenyl-4-sulfonylamino]-3-methylbutyric acid against MMP-3 and provided a 9-fold difference in their binding affinity. Such a result was proposed as due to different conformational entropy penalties accompanying their complexation. Moreover, on the basis of a different ΔC_p values for the binding of the two isomers, the authors propose the presence of water-mediated "bridging" hydrogen bonds within the S_1' subsite in the *R*-isomer complex. Our results are in agreement with both their conclusions and offer an insight at molecular level of the differences of their dynamical behavior.

Conclusions

On the basis of the structures of the MMP-8:*R* and MMP-8:*S* crystal complexes,[37] the higher activity of the *R*-isomer was mainly attributed to the presence in the latter of a direct inhibitor to enzyme H-bond between the sulfonamide NH and the A161 CO group, replacing a water-mediated H-bond with the P217 CO in the *S*-isomer, and to more extensive π-stacking interactions formed by both phenyl rings of the *R*-isomer with the H197 imidazole ring.

MD simulations of the fully hydrated complexes show that the sulfonamide NH gives a direct inhibitor to enzyme H-bond in both cases. Moreover the aromatic rings, forming π-stacking in the crystal state, were found to be mainly involved in the formation of weak interactions with water molecules. This finding is not surprising considering that the degree of hydration into the S_1' subsite, which is larger than in the crystal, competes with π-stacking interactions. Therefore, the differences between the two enantiomers, emerging from MD simulations, can essentially be ascribed to the diverse effects arising from the insertion of the biphenyl substituent into the S_1' subsite.

The biphenyl group of the *R*-isomer causes the breaking of the intramolecular R222 $N^{\eta}\cdots$P211 CO H-bond. This results in an increased mobility of the loops which were intramolecularly H-bonded, allows the biphenyl group to adopt two different conformations, and facilitates the bulk water entry and thus a higher degree of hydration and faster water exchange. On the contrary, the biphenyl group of the *S*-isomer maintains the R222 $N^{\eta}\cdots$P211 CO H-bond leading to a lower local enzyme flexibility. The biphenyl group is thus constrained in a single conformation, and the bulk water entry is hindered, so that the hydration degree is smaller than for the *R*-isomer.

MD results suggest that a decrease of the conformational entropy of the systems takes place upon complexation. However, the loss of entropy produced by the two enantiomers is significantly different. In the case under study, a more pronounced conformational entropy penalty accompanies not only the enzyme and the *S*-inhibitor but also the water molecules that, once trapped into the H-bonding network inside the active cavity, have a reduced capacity to fluctuate among energetic states, further decreasing the conformational entropy of the system. Therefore, in the light of the present study, the more extensive loss of conformational entropy in the S_1' subsite upon binding seems to be the major contribution to the lower affinity of the *S*-isomer.

The possibility of extensive conformational entropy changes involving the ligand−enzyme binding is an important factor determining the selectivity profile of the two enantiomers and should also be taken into account for the evaluation of binding affinities by computational methods.

Acknowledgment. We would like to acknowledge Prof. Alfredo Di Nola (Università di Roma 'La Sapienza') and Dr. Andrea Amadei (Università di Roma 'Tor Vergata') for helpful discussions.

References

(1) Shapiro, S. D. Matrix metalloproteinase degradation of extracellular matrix: Biological consequences. *Curr. Opin. Cell Biol.* **1998**, *10*, 602−608.
(2) Whittaker, M.; Floyd, C. D.; Brown, P.; Gearing, J. H. Design and Therapeutic application of matrix metalloproteinase inhibitors *Chem. Rev.* **1999**, *99*, 2735−2776.
(3) Gijbels, K.; Galardy, R. E.; Steiman, L. Reversal of experimental autoimmune encephalomyelitis with a hydroxamate inhibitor of metalloproteases. *J. Clin. Invest.* **1994**, *94*, 2177−2182.
(4) Chandler, S.; Coates, R.; Gearing, A.; Lury, J.; Wells, G.; Bone, E. Matrix metalloproteinase degrade myeline basic protein. *Neurosci. Lett.* **1995**, *201*, 223−226.
(5) Steinman, L. Multiple sclerosis: a coordinated immunological attack against myelin in the central nervous system. *Cell* **1996**, *85*, 299−302.
(6) Hewson, A. K.; Smith, T.; Leonard, J. P.; Cuzner, M. L. Suppression of experimental allergic encephalomyelitis in the Lewis rat by the matrix metalloproteinase inhibitor. *Inflamm. Res.* **1995**, *44*, 345−349.
(7) Lohmander, L. S.; Hoerrner, L. A.; Lark, M. W. Metalloproteinases, tissue inhibitor, and proteoglycan fragments in knee synovial-fluid in human osteoarthritis. *Arthritis Rheum.* **1993**, *36*, 181−189.
(8) Ahrens, D.; Koch, A. E.; Pope, R. M.; Stein-Picarella, M.; Niedbala, M. J. Expression of matrix metalloproteinase 9 (96-kd gelatinase B) in human rheumatoid arthritis. *Arthritis Rheum.* **1996**, *39*, 1576−1587.
(9) Blaser, J.; Friebel, S.; Maasjosthusmann, U.; Romisch, J.; Krahl-Mateblowski, U.; Freudenberg, W.; Fricke, R.; Tschesche, H. Detrmination in metalloproteinases, plasminogen-activators and their inhibitors in the synovial fluids of patients with rheumatoid arthritis during chemical synoviorthesis. *Clin. Chim. Acta* **1996**, *244*, 17−33.
(10) Ohishi, K; Fujita, N.; Morinaga, Y.; Tsuruo, T. H-31 human breast cancer cells stimulate type I collagenase production in osteoblast-like cells and induce bone resorption. *Clin. Exp. Metastasis* **1995**, *13*, 287−295.
(11) Witty, J. P.; Foster, S. A.; Stricklin, J. P.; Matrisian, L. M.; Stern, P. H. Parathyroid hormone-induced resorption in fetal rat limb bones is associated with production of the metalloproteinases collagenase and gelatinase B *J. Bone Miner. Res.* **1996**, *11*, 72−78.
(12) Peress, N.; Perillo, E.; Zucker, S. Localization of tissue inhibitor of matrix metalloproteinases in Alzheimer's disease and normal brain. *J. Neuropathol. Exp.Neurol.* **1995**, *54*, 16−22.
(13) Chang, C.; Werb, Z. The many faces of metalloproteinases: Cell growth, invasion, angiogenesis and metastasis. *Trends Cell Biol.* **2001**, *11*, S37−S43.
(14) Overall, C. M.; Lopez-Otin, C. Strategies for NMP inhibition in cancer: Innovations for the post-trial era. *Nat. Rev. Cancer* **2002**, *2*, 657−672.
(15) Coussens, L. M. Fingleton, B.; Matrisan, L. M. Matrix metalloproteinases inhibitors and cancer: Trials and tribulations. *Science* **2002**, *295*, 2387−2392.
(16) White, A. D. Emerging therapeutic advances for the development of second generation matrix metalloproteinase inhibitors. *Curr. Pharm. Des.* **1997**, *3*, 45−48.
(17) Babine, R. E.; Bender, S. L. Molecular Recognition of protein-ligand complexes: Application to drug-design. *Chem. Rev.* **1997**, *97*, 1359−1472.
(18) Puerta, D. T.; Cohen, S. M. A bioinorganic perspective of matrix metalloproteinase inhibition. *Curr. Top. Med. Chem.* **2004**, *4*, 1551−1573.
(19) Matter, H.; Schudok, M. Recent advances in the design of matrix metalloproteinase inhibitors. *Curr. Opin. Drug Discuss.* **2004**, *7*, 513−535.
(20) Bode, W.; Reinemer, P.; Huber, R.; Kleine, T. Schnierer, S.; Tschesche, H. The x-ray structure of catalytic domain of human neutrophil collagenase inhibited by a substrate analog reveals the essential for catalysis and specificity. *EMBO J.* **1994**, *13*, 1263−1269.
(21) Lovejoy, B. Structure of the catalytic domain of fibroblast collagenase complexed with an inhibitor. *Science* **1994**, *263*, 375−377.
(22) Borkakoti, N.; Winkler, F. K.; Williams, D. H.; D'Arcy, A.; Broadhurst, M. J.; Brown, P. A.; Johnson, W. H.; Murray, E. J. Structure of the catalytic domain of human fibroblast collagenase complexed with an inhibitor. *Nature Struct. Biol.* **1994**, *1*, 106−110.
(23) Gooley, P. R.; O'Connell, J. F.; Marcy, A. The NMR structure of the inhibited catalytic domain of the human stromelysin-1 *Nature Struct. Biol.* **1994**, *1*, 111−118.
(24) Stams, T.; Spurlino, J. C.; Smith, D. L.; Wahl, R. C.; Ho, T. F.; Qoronfleh, M. W.; Banks, T. M.; Rubin, B. Structure of human neutrophil collagenase reveals large S_1' specificity pocket. *Nature Struct. Biol.* **1994**, *1*, 119−123.
(25) Spurlino, J. C.; Smallwood, A. M.; Carlton, D. D.; Banks, T. M.; Vavra, K. J.; Johnson, J. S.; Cook, E. R.; Falvo, J.; Wahl, R. C. 1.56 Å structure of mature truncated human fibroblast collagenase. *Proteins: Struct. Funct. Genet.* **1994**, *19*, 98−109.
(26) Van Doren, S. R.; Kurochkin, A. V.; Hu, W.; Ye, Q.-Z.; Johnson, L. L.; Hupe, D. J.; Zuiderweg, E. R. P. Solution structure of the catalytic domain of human stromelysin complexed with a hydrophobic inhibitor. *Protein Sci.* **1994**, *4*, 2487−2498.
(27) Gonnella, N.; Bohacek, R.; Zhang, X.; Kolossvary, L.; Paris, C. G.; Melton, R.; Winter, C.; Hu, S.-L.; Ganu, V. Bioactive conformation of stromelysin inhibitors determined by transferred nuclear Overhauser effect. *Proc. Natl. Acad. Sci. U.S.A.* **1995**, 92, 462−466.
(28) Dhanarai, V.; Ye, Q. Z.; Johnson, L. L.; Hupe, D. J.; Ortwine, D. F.; Dunbar, J. B., Jr.; Rubin, J. R.; Pavlovsky, A.; Humblet, C.; Blundell, T. L. X-ray structure of a hydroxamate inhibitor complex of stromelysin catalytic domain and its comparison with members of the zinc metalloproteinase superfamily. *Structure* **1996**, *4*, 375−386.
(29) Moy, F. J.; Seddon, A.; Boehlen, P.; Powers, R. High resolution solution structure of basoc fibroblast prowth factor determined by multidimensional heteronuclear magnetic resonance spectroscopy. *Biochemistry* **1996**, *35*, 13552−13561.
(30) Moy, F. J.; Chanda, P. K.; Chen, J. M.; Cosmi, S.; Edris, W.; Skotnicki, J. S.; Wilhelm, J.; Powers, R. NMR solution structure of the catalytic fragment of human fibroblast collagenase complexed with a sulphonamide derivative of a hydroxamic acid compound. *Biochemistry* **1999**, *38*, 7085−7096.
(31) Lovejoy, B; Welch, A. R.; Carr, S.; Luong, C.; Broka, C.; Hendricks, R. T.; Campbell, J. A.; Walker, K. A. M.; Martin, R.; Van Wart, H.; Browner, M. F. Crystal Structures of MMP-1 and -13 reveal the structural basis for selectivity of collagenase inhibitors. *Nature Struct. Biol.* **1999**, *6*, 217−221.

(32) Zhang, X.; Gonnella, N.; Koehn, J.; Pathak, N.; Ganu, V.; Melton, R.; Parker, D.; Shu-Ih, H.; Ki-Yean, N. Solution structure of the catalytic domain of human collagenase-3 (MMP-13) complexed to a potent non-peptidic sulphonamide inhibitor: binding comparison with stromelysin-1 and collagenase-1. *J. Mol. Biol.* **2000**, *301*, 513−524.

(33) D'Alessio, S.; Gallina, C.; Gavuzzo, E.; Giordano, C.; Gorini, B.; Mazza, F.; Paradisi, M. P.; Panini, G.; Pochetti, G.; Sella, A. Inhibition of adamalysin II and MMPs by phosphonate analogues of snake venom peptides. *Bioorg. Med. Chem.* **1999**, *7*, 389−394.

(34) Gavuzzo, E.; Pochetti, F.; Mazza, F.; Gallina, C.; Gorini, B.; D'Alessio, S.; Pieper, M.; Tschesche, H.; Tucker, P. A. Two crystal structures of human neutrophil collagenase, one complexed with a primed and the other with an unprimed-side inhibitor. Implications for drug design. *J. Med. Chem.* **2000**, *43*, 3377−3385.

(35) Bianchini, G.; Aschi, M.; Cavicchio, G.; Crucianelli, M.; Preziuso, S.; Gallina, C.; Nastri, A.; Gavuzzo, E.; Mazza, F. Design, modelling synthesis and biological evaluation of peptidomimetic phosphinates as inhibitors of matrix metalloproteinases MMP-2 and MMP-8. *Bioorg. Med. Chem.* **2005**, *13*, 4740−4749.

(36) Campestre, C.; Agamennone, M.; Tortorella, P.; Preziuso, S.; Biasone, A.; Gavazzo, E.; Pochetti, G.; Mazza, F.; Hiller, O.; Tschesche, H.; Consalvi, V.; Gallina, C. N-Hydroxyurea as zinc binding group in matrix maetalloproteinase inhibition: Mode of binding in a complex with MMP-8. *Bioorg. Med. Chem. Lett.* **2006**, *16*, 20−24.

(37) Pochetti, G; Gavuzzo, E.; Campestre, C.; Agamennone, M.; Tortorella, P.; Consalvi, V.; Gallina, C.; Hiller, O.; Tschesche, H.; Tucker, P.; Mazza, F. Structural insight into the stereoselective inhibition of MMP-8 by enantiomeric sulfonamide phosphonate. *J. Med. Chem.* **2006**, *49*, 923−931.

(38) Parker, M. H.; Ortwine, D. F.; O'Brien, P. M.; Lunney, E. A.; Banotai, C. A.; Mueller, W. T.; McConnell, P.; Brouillette, C. G. Stereoselective binding of an enantiomeric pair of stromelysin-1 inhibitors caused by conformational entropy factors. *Bioorg. Med. Chem. Lett.* **2000**, *10*, 2427−2430.

(39) O'Brien, P. M.; Ortwine, D. F.; Pavlovsky, A. G.; Picard, J. A.;Sliskovic, D. R.; Roth, B. D.; Dyer, R. D.; Johnson, L. L.; Man, C. F.; Hallak, H. Structure-activity relationships and pharmacokinetic analysis for a series of potent, systemically available biphenylsulfonamide matrix metalloproteinase inhibitors. *J. Med. Chem.* **2000**, *43*, 156−166.

(40) Aschi, M.; Roccatano, D.; Di Nola, A.; Gallina, C.; Gavuzzo, E.; Pochetti, G.; Pieper, M.; Tschesche, H.; Mazza, F. Computational study of the catalytic domain of human neutrophil collagenase. Specific role of S3 and S′3 subsites in the interaction with a phosphonate inhibitor. *J. Comput.-Aided Mol. Des.* **2002**, *16*, 213−225.

(41) Jarymowycz, V. A.; Stone, M. J. Fast time scale dynamics of protein backbones: NMR relaxation methods, application and functional consequences. *Chem. Rev.* **2006**, *106*, 1624−1671.

(42) Adcock, S. A.; Mc Cammon, J. A. Molecular Dynamics: survey of methodsfor simulating the activity of proteins. *Chem. Rev.* **2006**, *106*, 1589−1615.

(43) Stone, M. J. NMR relaxation studies of the role of conformational entropy in protein stability and ligand binding. *Acc. Chem. Res.* **2001**, *34*, 379−388.

(44) Van der Spoel, D.; van Buren, A. R.; Apol, E.; Meulenhoff, P. J.; Tieleman, D. P.; Sijbers, A. L. T. M.; van Drunen, R.; Berendsen, H. J. C. Gromacs User Manual version 1.3, 1996.

(45) Berendsen, H. J. C.; Postma, J. P. M.; van Gunsteren, W. F. Hermans Interaction models for water in relation to protein hydration. In *Intermolecular Forces*; Pullman, B., Ed.; D. Reidel Publishing Company: Dordrecht, 1981; pp 331−342.

(46) Amadei, A.; Chillemi, G.; Ceruso, M.; Grottesi, A.; Di Nola, A. Molecular dynamics simulations with constrained roto-translational motions: theoretical basis and statistical mechanical consistency. *J. Chem. Phys.* **2000**, *112*, 9−23.

(47) **(**47) Berendsen, H. J. C.; Postma, J. P. M.; van Gunsteren, W. F.; Di Nola, A. Molecular Dynamics with coupling to an external bath. *J. Chem. Phys.* **1984**, *81*, 3684−3690.

(48) Hess, B.; Bekker, H.; Berendsen, H. J. C.; Frajie, J. G. E. M. LINCS: a linear constraint solver for molecular simulations. *J. Comput. Chem.* **1997**, *18*, 1463−1472.

(49) Darden, T. A.; York, D. M.; Pedersen L. G. Particle mesh Ewald: method for Ewald sums in large systems. *J. Chem. Phys.* **1993**, *98*, 10089−10092.

(50) van Gunsteren, W. F.; Billeter, S. R.; Eising, A. A.; Hunemberger, P. H.; Kruger, P.; Mark, A. E.; Scott, V. R. P.; Tironi, I. G. *Biomolecular simulations: The GROMOS96 manual and user guide*; vdf Hochschlverlag AG an der ETH Zurich: Zurich, 1996.

(51) Breneman, C. M.; Wiberg, K. B. Determining atom-centered monopoles from molecular electrostatic potentials. *J. Comput. Chem.* **1990**, *11*, 361−367.

(52) Parr, R. G.; Yang, W. *Density functional theory of atoms and molecules*; Oxford University Press: New York, 1989.

(53) Schmidt, M. W.; Baldridge, K. K.; Boatz, J. A.; Elbert, S. T.; Gordon, M. S.; Jensen, J. J.; Koseki, S.; Matsunaga, N.; Nguyen, K. A.; Su, S.; Windus, T. L.; Dupuis, M.; Montgomery, J. A. General Atomic and Molecular Electronic Structure System *J. Comput. Chem.* **1993**, *14*, 1347−1363.

(54) Amadei, A.; Linssen, A. B. M.; Berendsen, H. J. C. Essential dynamics of proteins. *Proteins: Struct., Funct. Genet.* **1993**, *17*, 412−425.

(55) Stocker, W; Grams, F.; Baumann, U.; Reinemer, P.; Gomis-Ruth, F. X.; McKay, D. B.; Bode, W. The metzincins : topological and sequential relations between the astacins, adamalysins, serralysins, and matrixins define a superfamily of zinc-peptidases. *Protein Sci.* **1995**, *4*, 823−840.

(56) Carney, C. F. F.; Ferrara, J. E.; Brunner, S. Methods for computing protein binding affinity *J. Comput. Chem.* **2005**, *26*, 243−251.

(57) McCammon, J. A. Theory of biomolecular recognition *Curr. Opin. Struct. Biol.* **1998**, *8*, 245−249.

(58) Simonson, T.; Archontis, G.; Karplus, M. Free energy simulation come of age: protein-ligand recognition. *Acc Chem. Res.* **2002**, *35*, 430−437.

(59) Ajai, A.; Murcko, M. Computational methods to predict free energy in ligand receptor complexes. *J. Med. Chem.* **1998**, *38*, 4953−4967.

(60) Swanson, J. M. J.; Henchman, R. H.; McCammon, J. A. Revisiting free energy calculations: a theoretical connection to MM/PBSA and direct calculation of the association free energy. *Biophys. J.* **2004**, *86*, 67−74.

JM0608457